Published in final edited form as:
JACC Cardiovasc Imaging. 2012 November ; 5(11): 1127–1138. doi:10.1016/j.jcmg.2012.01.025.

Selective factor XIIa inhibition attenuates silent brain ischemia

John W. Chen, MD, PhD[1,*], **Jose-Luiz Figueiredo, MD**[1,*], **Gregory R. Wojtkiewicz, MS**[1,*], **Cory Siegel, BS**[1], **Yoshiko Iwamoto, BS**[1], **Dong-Eog Kim, MD**[2], **Marc W. Nolte, PhD**[3], **Gerhard Dickneite, PhD**[3], **Ralph Weissleder, MD, PhD**[1], and **Matthias Nahrendorf, MD, PhD**[1]

[1]Center for Systems Biology, 185 Cambridge Street, Boston, MA 02114

[2]Division of Stroke Medicine, Department of Neurology, Dongguk University Ilsan Hospital, 814 Siksa-dong, Goyang, Republic of Korea

[3]CSL Behring GmbH, 35002 Marburg, Germany

Abstract

Objective—To use molecular imaging targeting coagulation pathway and inflammation to 1) better understand the pathophysiology of silent brain ischemia (SBI) and 2) monitor the effects of factor XIIa inhibition.

Background—Silent brain ischemia can be observed in patients who undergo invasive vascular procedures. Unlike acute stroke, the diffuse nature of SBI and its less tangible clinical symptoms make this disease difficult to diagnose and treat.

Methods—We induced SBI in mice by intra-arterial injection of fluorescently-labeled microbeads or fractionated clot into the carotid artery. After SBI induction, diffusion-weighted (DWI) magnetic resonance imaging (MRI) was performed to confirm the presence of microinfarcts in asymptomatic mice. Molecular imaging targeting the downstream factor XIII activity (SPECT-CT) at three hours and myeloperoxidase activity (MRI) on day three after SBI induction were performed, without and with the intravenous administration of a recombinant selective factor XIIa inhibitor derived from the hematophagous insect Triatoma infestans (rHA-Infestin-4). Statistical comparisons between two groups were evaluated by the Student's t-test or the Mann-Whitney U test.

Results—In SBI-induced mice, we found abnormal activation of the coagulation cascade (factor XIII activity) and increased inflammation (myeloperoxidase activity) close to where emboli lodge in the brain. rHA-Infestin-4 administration significantly reduced ischemic damage (53–85% reduction of infarct volume, $p < 0.05$) and pathological coagulation (35–39% reduction of factor XIII activity, $p < 0.05$) without increasing hemorrhagic frequency. Myeloperoxidase activity, when normalized to the infarct volume, did not significantly change with rHA-Infestin-4 treatment, suggesting that this treatment does not further decrease inflammation other than that resulted from the reduction in infarct volume.

Address for correspondence: Matthias Nahrendorf, Center for Systems Biology, 185 Cambridge Street, Boston, MA 02114, Tel: (617) 643-0500, Fax: (617) 643-6133, mnahrendorf@mgh.harvard.edu.
*These authors contributed equally

Disclosures

G.D. and M.W.N. are employees of CSL Behring GmbH. G.D. owns employee shares of CSL Limited. The remaining authors have no disclosures.

Conclusions—Focal intracerebral clotting and inflammatory activity are part of the pathophysiology underlying SBI. Inhibiting factor XIIa with rHA-Infestin-4 may present a safe and effective treatment to decrease the morbidity from SBI.

Keywords

Silent brain ischemia; coagulation; inflammation; imaging; infestin

INTRODUCTION

Behavioral changes, neuropsychological deficits and aggravated vascular dementia can be observed in patients after cardiovascular surgery (e.g. coronary bypass surgery, valve replacement, carotid endarterectomy) and in patients undergoing vascular interventions (1). With the advent of sensitive imaging modalities such as diffusion weighted MRI, there has been an increasing awareness of injury to the brain in patients without major symptoms. These lesions, called “silent brain ischemia” (SBI), are thought to be caused by microembolism from debris, air, fat, or fragmented thrombi (2, 3). The overall incidence in the general patient population is 2–3%, with a prevalence increasing with age of up to 20% in the elderly (3, 4). Vascular procedures, such as angiography, carotid endarectomy and stenting, and heart surgery can increase the risk for SBI substantially (1, 3). The presence of SBI has also been found to be associated with dementia and increased risk of stroke (4). Currently, no effective therapy exists for treating this condition.

In this work, we reasoned that coagulation factor XII (FXII) can serve as a potential therapeutic target in SBI. FXII is a serine protease that initiates the intrinsic coagulation cascade by activation of FXI to FXIa (5) and also has immune-modulatory functions (6). It binds an Fc receptor on monocytes, increases release of IL-1 and IL-6 from monocytes and macrophages and stimulates neutrophils (7–9). FXII also activates chemerin, a chemoattractant that binds a G-protein coupled receptor on dendritic cells and macrophages, directing an immune response to the site of injury (10). Additionally, FXII activates prekallikrein and thus bradykinin formation, which in turn is a potent inflammatory mediator that induces vasodilation and vascular leakage (11). FXII deficient mice have decreased plasma bradykinin levels, suggesting that FXII may ameliorate a potentially harmful inflammatory response that can cause further damage (12, 13). It has been suggested that FXII improves the strength and size of a developing thrombus (11). Interestingly, deficiency or inhibition of FXII protects against arterial thrombus formation and reduces cerebral injury in mouse models of stroke without increasing the risk of bleeding (14, 15). In humans, hereditary deficiency of FXII is not associated with abnormal bleeding diathesis (16). That a FXII-driven pathway is required for pathologic thrombus formation but is not involved in hemostasis suggests that FXII inhibition could be a promising and safe therapeutic strategy (17, 18) for SBI.

Infestins are a class of serine protease inhibitors derived from the midgut of the hematophagous insect, Triatoma infestans, a major vector for the parasite Trypanosoma cruzi, known to cause Chagas’ disease (19). The insect uses these inhibitors to prevent coagulation of ingested blood. The Infestin gene encodes 4 domains that express proteins inhibiting different factors in the coagulation pathway (19), including Infestin-4, a strong inhibitor of activated coagulation factor XII (FXIIa). In this study, we found that rHA-Infestin-4 (recombinant Infestin-4, fused to human albumin for prolongation of blood half-life) decreased the amount of ischemic injury in both a thromboembolic and in a microbead embolic model that mimics SBI caused by other materials such as air or fat. We used two targeted molecular imaging approaches to a) examine treatment effects on the coagulation cascade by imaging activity of the downstream clotting factor XIIIa and b) study brain

inflammation by magnetic resonance imaging of myeloperoxidase (MPO) activity. We found that in murine SBI, microembolism caused clotting and inflammation in the brain, and that rHA-Infestin-4 reduced micro-infarctions through anti-coagulatory effects without changing the inflammatory response.

METHODS

Mice

All experiments were performed in adult Balb/c mice obtained from Charles River Laboratories, Inc. (Wilmington, MA). Thirty-six mice were used to optimize the animal model with respect to surgical access and the type and amount of injected materials. The Institutional Review Board approved all animal experiments. Mice were anesthetized in an isoflurane chamber with 2% isoflurane by inhalation with 2L/min of supplemental oxygen and transferred to a warm heating pad in a supine position while under isoflurane.

Most likely, SBI in patients is caused by a shower of minuscule emboli that lodge in the small vessels in the brain and result in diffuse ischemic injury, while large-scale blood flow is not interrupted. Therefore, to leave the internal carotid artery intact, we chose to retrogradely inject embolic material into the external carotid artery. Thromboemboli and microbeads were injected one-sided through the external carotid artery into the internal carotid artery while the common carotid artery was temporarily occluded. This forced the emboli into the arterial system of the brain without compromising perfusion. 8-0 Ethicon mononylon sutures (Johnson & Johnson, Brussels, Belgium) were used for all arterial ligations. A temporary ligation was made on the common and on the internal carotid artery to stop the blood flow during catheter placement. The distal suture around the external carotid artery was permanently tied off and a second suture was placed around the artery to secure the catheter. The external carotid artery was opened 5 mm distal of the carotid bifurcation. We then inserted a modified intramedic polyethylene PE10 catheter (I.D. 0.28mm, I.D. 0.61mm, Becton Dickinson and Company, Sparks, MD) retrogradely into the external carotid artery, with the tip of the catheter facing the bifurcation (Fig. 1). The ligation on the internal carotid artery was then released allowing for flow of injected material into the internal carotid artery. Flashback of arterial blood into the catheter was observed, and then either microbeads or thromboemboli were injected. In a control group, we only ligated the external carotid artery, which did not lead to ischemic injury of the brain. After injection of emboli, the catheter was removed and the external carotid artery was ligated to stop bleeding. The ligatures at the internal carotid and common carotid arteries were removed to re-establish arterial flow, and the wound was closed with 7-0 nylon suture.

Fluorescent microbeads

After optimization experiments, we found that intracarotid injection of 500 microbeads of 43 μm diameter resulted in reproducible, clinically silent micro-lesions. A syringe loaded with 500 Fluoresbrite™ Plain YG 45 Microspheres (Polysciences, Inc., Warrington, PA, excitation/emission 441 nm/486 nm) was attached to the catheter to inject the beads (Fig. 1).

Fluorescent thromboemboli

500μL of fresh mouse blood was withdrawn from donor mice via cardiac puncture and immediately added to sodium citrate solution for initial anticoagulation (final concentration, 0.32%). After centrifugation at 1500 rpm for 10 minutes to remove cells, 20 μmol $CaCl_2$ and 10 units of high activity human thrombin was added to the plasma to induce clotting (Calbiochem, EMD Chemicals, Inc., Darmstadt, Germany, MW 37,000, 100 units/mL, specific activity 2800 NIH units/mg protein). To label the thromboemboli, 2nmol of

Genhance 680 (Perkin Elmer, MA) was added. The material was stored at 4°C for up to 72 hours. Before use, the clot was washed with normal saline and treated with a tissue homogenizer to fractionate the clot into small particles ~10 μm in diameter (Fig. 1). Optimization experiments determined that a volume of 10 μL of this preparation did not cause overt neurological deficits.

The above emboli sizes were chosen to better account for the variability of different types of injury that may occur in the clinical setting. The human middle cerebral artery (MCA) is about 4 mm in diameter, with large emboli considered to be those greater than 2 mm in size. Mouse MCA is about 80 microns in diameter. Therefore, we chose two types of emboli that can be considered small (10 microns) and relatively large (43 microns, just over 50% of the diameter of mouse MCA).

Stroke Assessment

After recovery from anesthesia, mice were assessed for signs of stroke using the Benderson scale (20) after SBI induction. We also observed the animals for dyskinesia, lethargy, grip, limb weakness, eyelid droop, gait disturbance, circling, and rolling. Observation of any of the above symptoms was considered to be an indicator of stroke, while lack of the above symptoms and a Benderson score of 0 (normal) indicated that no overt stroke had occurred, consistent with the possibility of SBI. If no stroke symptoms were present, the mice were used for this study; otherwise they were excluded. A total of 4 mice were excluded after thromboembolism and 7 mice after microbeads injection.

Study groups

After optimization of the animal model, we proceeded to study 4 cohorts (n = 5–9 per group): Mice with induction of SBI by thromboemboli or microbeads (untreated controls), and 2 additional groups in which mice were treated with rHA-Infestin-4 (CSL Behring GmbH) at a dose of 200mg/kg via intravenous tail vein injection. The mice received their first injection immediately after SBI induction. Single Photon Emission Computed Tomography – X-ray Computed Tomography (SPECT-CT) imaging of FXIII activity was done 3 hours after SBI. The cohorts that were imaged three days after SBI by MRI received daily injections until and including on day 3 after injury. 2,3,5, triphenyltetrazolium chloride (TTC) staining was assessed 3 days after SBI to measure the microinfarct burden.

MRI for assessment of infarct volume and myeloperoxidase activity

MRI was performed using a Bruker 4.7T scanner with a RARE T1 sequence (TR 1500 ms, TE 8 ms, averages 8, matrix: 192 × 192 × 22, Voxel size: 0.133mm × 0.13 mm × 0.5 mm); and a RARE T2 sequence with the same geometry (TR 5622ms, TE 20 ms, averages 4). To evaluate the model, we also used diffusion weighted imaging (DWI) after SBI induction. An EPI diffusion weighted sequence with 6 diffusion directions was employed (TR:4800 ms, TE: 32ms, Matrix: 128 × 128 × 22, Voxel Size: 0.195 mm × 0.195 mm × 0.5 mm).

Myeloperoxidase (MPO) is an abundant enzyme secreted by many inflammatory myeloid cells such as neutrophils, Ly-6C^{high} monocytes, subsets of activated macrophages and microglia during inflammation, and thus is a suitable imaging biomarker for the local inflammatory response. Mice were scanned before and 90 min after intravenous administration of 0.3 mmol/kg of myeloperoxidase-gadolinium contrast agent (MPO-Gd) (21–23) 3 days after SBI induction. MPO-Gd is a gadolinium-encaging chelator (DTPA) derivatized with 2 serotonin moieties, and can react with other MPO-Gd molecules to form oligomers in tissue with high MPO activity, but remain as single molecules in the absence of MPO activity (21, 28). MPO-Gd causes highly MPO-specific tissue enhancement (22, 23). After imaging, mice were sacrificed, perfused with normal saline and the brains were

harvested and sliced for fluorescence imaging on a mesoscopic fluorescent imager (OV-100, Olympus) to verify that emboli were present.

Amira (Visage Imaging, San Diego, CA) and Matlab (MathWorks, Natick, MA) software was used for data analysis. T2 images were segmented by region-based thresholding for volume computation and 3D visualization of lesions. Regions of interest (ROI's) were identified on each image slice of the 90 minute post injection T1 scans. The brain ventricles were excluded by manual segmentation of T2 images prior to automated segmentation of MPO-Gd positive areas on T1 scans. MPO-Gd positive voxels were quantitated by a Matlab procedure that counted voxels with a signal intensity that was 3 standard deviations above the average signal in normal brain tissue. To determine whether Infestin has additional effects on inflammation, the MPO-Gd positive volume was normalized to the T2 volume to account for change in infarct size. In addition, we quantified the contrast to noise ratio (CNR), which reflects the degree of inflammation in tissue (22, 23). This approach has been validated previously, including imaging in $MPO^{-/-}$ mice (22).

SPECT-CT for assessment of clotting cascade activation

Because cross-linking of fibrin by FXIII is considered the final step in the formation of a clot, it is a useful measure of overall clotting activity. We performed in vivo SPECT-CT imaging using the FXIII-specific molecular probe FXIII-Ind (24, 26) during the acute stage after SBI induction. This imaging agent consists of an Indium-111 labeled peptide that is recognized by FXIII as specific substrate and is then incorporated into the forming clot. Previous work carefully characterized the specificity of the imaging agent using a scrambled peptide sequence (27) and $FXIII^{-/-}$ mice (26). Four groups of mice underwent SBI induction and treatment one hour prior to injection of approximately 1 mCi of a factor XIII-substrate peptide labeled with Indium-111 (actual amount injected was 731–1273 μCi). SPECT-CT was performed using the Gamma Medica-Ideas X-SPECT small animal imaging system. We used a cone beam (50 kVp, 500 mA) x-ray tube with a solid state CMOS detector over 256 projections. These projections were reconstructed using the modified feldkamp reconstruction algorithm. The SPECT scan utilized dual gamma cameras with 1 mm medium energy pinhole collimators through 64 projections (32 projections from each camera) at 90 s/projection. The SPECT images were reconstructed using the ordered subsets expectation maximization algorithm (OSEM) and fused to the CT images for accurate anatomical colocalisation of molecular information.

Animals were sacrificed immediately after SPECT-CT imaging. The brain was excised and tissue analyzed with a Wallac Wizard 1480 gamma well counter. Afterwards, the brain was sliced into 2 mm thick sections and imaged by FRI as described below to verify presence of fluorescent emboli. Afterward the tissue slices were placed on phosphorimager plates overnight for autoradiography and analyzed on a Molecular Dynamics Typhoon phosphor imager plate reader.

For SPECT-CT data analysis, the entire brain and skeletal muscle were manually segmented from the CT images using Amira software to calculate the target to background ratio (TBR), with muscle activity serving as background. Data were normalized for the mass of the brain and the injected dose of each animal. Autoradiography and gamma counting data were decay corrected to the time of sacrifice. 3D visualizations of the SPECT-CT data were rendered using Osirix software (Geneva, Switzerland).

Ex Vivo imaging and pathology

After sacrifice, the brain was cut into 2 mm thick coronal sections using a mouse brain slicer (Zivic Instruments, Pittsburgh, PA) and imaged with an OV-100 small animal imaging

system (Olympus, Center Valley, PA), a hybrid of a planar reflectance fluorescence imaging system and a high-power microscope. The brain sections were imaged using the GFP fluorescence channel (excitation 400nm, emission 508nm) for the microbeads and the near-infrared channel for the fluorescent thromboemboli (excitation 680nm) with up to 16-times magnification. White light images were also acquired to assess potential hemorrhage caused by injury.

For assessment of microinfarct burden three days after SBI, brain slices were produced and placed into a 1% TTC in PBS solution for 30 minutes at 37°C. The brain sections were then washed three times with PBS for one minute each and then imaged using a digital camera (Olympus FE-280) to assess TTC staining. Viable brain tissue stained red with TTC while infarcted regions did not stain.

Histology

For further histological analysis, slices of brain tissue were embedded in O.C.T. compound (Sakura Finetek, Torrance, CA), and serial 5μm frozen sections were cut. The avidin-biotin peroxidase method was used for immunohistochemistry and tissue sections were incubated with Factor XIII A: C-20 (Santa Cruz Biotechnology, Inc., Santa Cruz, CA) followed by a biotinylated anti-goat IgG secondary antibody (Vector Laboratories, Inc., Burlingame, CA). The reaction was visualized with a 3-amino-9-ethylcarbazole (AEC) substrate (DakoCytomation, Carpinteria, CA) and all sections were counterstained with Harris hematoxylin solution. The slides were digitized automatically at magnification 400 and images were captured using NanoZoomer 2.0-HT (Hamamatsu, Japan).

Statistics

Results are expressed as mean ± SEM. Statistical comparisons between two groups were evaluated by Student's t-test or the Mann-Whitney U test (if the variances were significantly different between the two groups assessed by the F-test). A value of $p < 0.05$ was considered to indicate statistical significance.

RESULTS

A mouse model of SBI

We found that in 5 control mice, ligation of the external carotid artery and placement of the catheter but without injection of thrombogenic material did not cause ischemic injury. When these mice were imaged by SPECT-CT or MRI, we did not find injury sequela. Next we chose 2 different materials to mimic microembolism, accounting for the heterogeneous nature of SBI. Fluorescent microbeads of 43 μm diameter, as well as fractionated blood clots that were labeled with fluorochromes (~10 μm size), resulted in variable symptoms and degree of tissue damage, depending on the amount of material injected. In optimization experiments, we adjusted the quantity of embolic material to avoid neurologic deficits that are the hallmark of stroke, which we frequently found if >1000 microbeads or >30 μL of thromboembolic material were injected. Specifically, 500 microbeads and 10 μL of thromboembolic material rarely caused stroke-like symptoms, and we chose these quantities for all further experiments. If stroke symptoms occurred nevertheless, animals were excluded from the study.

Both embolic materials were fluorescent, thus we could observe how they produced occlusions in small cerebral vessels (Fig. 1A–C) and micro-infarctions in the brain. Fluorescent labeling of emboli also allowed us to locate them in the target tissue, thus fluorescence imaging served as quality control for the procedure in all subsequent experiments. Most emboli and subsequent molecular imaging signal was located in the

ipsilateral hemisphere, however; some spill over, likely through anastomoses provided by the Circle of Willis, was observed in the contralateral hemisphere. Diffusion weighted MRI showed the typical subtle changes that are described in human patients with SBI (Fig. 1D).

rHA-Infestin-4 administration reduces tissue damage in SBI

To assess the amount of brain tissue damage caused by emboli, we computed the percentage of the brain that is infarcted for each model from MRI (Fig 2A,B). We found both SBI models resulted in infarct volumes that are on average <4% of the brain volume, which are substantially less than the average infarct volume in human stroke patients that average about 9% (25). Interestingly, the microbeads model generated slightly larger average infarct volume compared to the thromboemboli model (3.5±1.3% versus 1.1±0.4%, $p = 0.09$). To corroborate the imaging data, we also performed TTC staining on slices that we had harvested from mice three days after embolization. Both types of micro-embolization produced small infarcts (Fig. 2C,D) that occupied < 5% of the brain by area, similar to the volume results from MRI. Again, we found that injection of microbeads produced slightly more tissue damage compared to the thromboemboli (4.9±0.9% versus 2.1±0.5%, $p = 0.06$).

When mice were treated with rHA-Infestin-4, significantly decreased micro-infarction was detected by MRI for both materials (microbeads model 53% reduction, thromboemboli model 85%, Fig. 2A,B). TTC staining further confirmed these findings (microbead model 54% reduction, thromboemboli model 66% reduction, Fig. 2C,D).

We found evidence of microhemorrhages in 6/8 (75%) of mice injected with microbeads and in 5/9 (56%) of mice injected with thromboemboli (Fig. 3). After rHA-Infestin-4 administration, occurrence of microhemorrhage did not increase. In fact, treatment reduced the occurrence of microhemorrhages from 75 to 67% in the bead model and from 55 to 12% in the clot model (p = n.s. and 0.07, respectively; Fig. 3).

rHA-Infestin-4 treatment decreases clotting secondary to SBI

To assess the effect of rHA-Infestin-4 on coagulation, we studied the activity of factor XIII, which is downstream from and affected by FXII and responsible for cross-linking fibrin clots. In mice with SBI, we found diffuse SPECT signal in the ipsilateral brain hemisphere, indicating that the injected micro-emboli induced intravascular coagulation once they lodged in the brain. The location of the SPECT signal was corroborated by ex vivo autoradiography, which also showed that activity co-localized with microbeads and thromboemboli on fluorescence reflectance images (Fig. 4 and 5).

There was significant reduction in the amount of factor XIII activity after rHA-Infestin-4 administration in both, SBI caused by injection of thromboemboli (Fig. 4) and microbeads (Fig. 5). This was corroborated by ex vivo autoradiography exposure of brain sections (middle panels of Figs. 4 and 5). The overall degree of factor XIII activity reduction is visualized on the 3D SPECT-CT images (Figs. 4 and 5, left panels). Immunohistochemical staining for FXIII confirmed in vivo imaging results (Fig. 6).

rHA-Infestin-4 does not alter myeloperoxidase activity in the brain after SBI

To assess MPO activity in vivo, we performed MR imaging three days after SBI using the molecular imaging agent MPO-Gd. In a cohort of normal mice, no enhancement was found after injection of MPO-Gd (data not shown). In mice with SBI, we found diffuse enhancement after injection of MPO-Gd, co-localizing with the embolic material on ex vivo fluorescence images (Figs. 7 and 8). Injection of microbeads induced more MPO activity when compared to thromboemboli (contrast-to-noise-ratio, CNR, microbeads: 36 ± 1,

thromboemboli: 23 ± 2, $p<0.05$) and larger lesions (number of MPO-Gd^+ voxels in the brain, microbeads: 3162 ± 1435, thromboemboli: 548 ± 207; $p = 0.05$).

In both models, there was a trend toward decrease in MPO-Gd+ volume after rHA-Infestin-4 treatment. Interestingly, after accounting for infarct volume, we found that the normalized MPO+ volume did not change after treatment (Figs. 7 and 8). The average CNR of MPO-positive lesions was also unchanged (Figs. 7 and 8).

DISCUSSION

Due to the absence of severe clinical signs and symptoms, SBI is a complication of medical procedures that is difficult to diagnose and therefore often overlooked. Increased use of DWI MRI has provided evidence that the incidence of SBI increases with age and with vascular procedures. There is no treatment available in the clinic. We employed a mouse model that reflects the heterogeneous pathophysiology of SBI by using microthrombi and microbead embolism to study sequelae of SBI with respect to intravascular activation of the coagulation system and the inflammatory response. Regardless of the material for the microemboli, in absence of stroke-like symptoms, we found activation of the clotting cascade in vicinity of the microemboli, measured by SPECT-CT imaging FXIII activity, a clotting factor that is involved in the final step of the coagulation cascade. We further detected increased inflammatory activity, reported by myeloperoxidase magnetic resonance imaging. Furthermore, we report that rHA-Infestin-4, a recombinant FXIIa inhibitor fused to human albumin for prolongation of its half-life, significantly reduced both, factor XIII activity and the burden of micro-infarction. These findings imply rHA-Infestin-4 as a potential treatment in patients diagnosed with SBI.

Clinicians frequently encounter neuropsychological symptoms in patients that underwent major cardiovascular interventions. Because conventional brain imaging techniques showed no anatomic correlates, these “subtle” changes in alertness, orientation, mood and character were often dismissed as difficulty to adjust to the hospital environment or advanced age. The advent of imaging techniques that have very high sensitivity such as DWI MRI has brought to light that an astounding number of patients have post-procedural impairment of diffusion in their brain (1, 3). Improving our understanding of SBI biology, we found that in mice after microembolization, regardless of the material of the emboli, there is considerable pathology even in the absence of stroke symptoms. Specifically, FXIII activity was increased 3 hours after embolization, indicating increased coagulation at the site where embolic material lodged. Three days later, these brain areas showed significant inflammation as a response to the tissue injury. We speculate that the arrest of blood flow in the smallest vessels in the brain after fragmented clot or beads lodged in them caused secondary clotting and ischemic death of small volumes of brain tissue, and in some cases microhemorrhages. Secondary intravascular clotting may thus serve as a therapeutic target, as seen in the mouse cohorts treated with rHA-Infestin-4. The described mouse model can be used for future studies of SBI, especially to test therapeutic approaches to prevent it. The use of fluorescent embolic material is advantageous because it can serve as a quality control for the procedure and informs on where the injected materials lodged, which is otherwise difficult to determine. Commercially available fluorescent microbeads proved particularly suitable, as the amount of injury can be standardized due to the homogenous size of beads and the ease of dosing. Limitations of the model include the observed microhemorrhages, which have not been reported in clinical cases of SBI. Future studies should also focus on long-term sequela and explore if these are comparable to the clinical situation.

We characterized SBI in mice using 2 molecular imaging approaches that are well positioned to detect subtle changes early in the course of disease. Myeloperoxidase activity

was imaged by MRI on day 3, when the inflammatory activity peaks in stroke (23). The increased MPO activity suggests that a response occurs that parallels stroke, specifically the recruitment of innate immune cells to the site of injury. At this point it is unclear if subsequent inflammation exacerbates ischemia of brain cells, and if it also could be targeted therapeutically. In the current study, rHA-Infestin-4 did not change the normalized MPO+ volume after accounting for infarct size, suggesting that this treatment did not have additional effects on inflammation other than from the decrease in infarct size. In addition, myeloperoxidase signal on day 3 after SBI was not changed by treatment. Thus, the MPO-Gd+ areas seen on imaging may represent “breakthrough” injured areas that escaped infestin treatment. As such, these areas did not demonstrate any change in MPO activity.

As early as 3 hours after induction of injury in our murine models, there was significant SPECT signal indicating heightened FXIII activity. Given the lack of overt symptoms in SBI, rtPA is likely not suitable for SBI. Even in stroke, patients with mild symptoms are not treated with thrombolytic therapy due to the substantial risk of hemorrhagic complications (29). Conversely, similar to previous studies on stroke (14, 17), FXII inhibition did not increase frequency of hemorrhage in SBI, pointing towards a favorable profile of unwanted side effects. In general, anticoagulatory therapy carries an increased risk of bleeding, and this would reduce enthusiasm for a therapy targeting SBI, which is not a life-threatening condition. However, this was not the case for rHA-Infestin-4. This finding is in line with the symptoms of hereditary FXII deficiency, which do not include inadequate bleeding. Altogether, the data suggest that FXII inhibition could serve as prophylactic therapy in high-risk cases, and may be safe in patients that undergo procedures involving arterial catheterization or vascular surgery. These hypotheses will have to be tested in future studies, especially as therapy was started 1 hour after embolization in our study.

Our findings in mice demonstrate that in SBI both coagulation and inflammatory pathways are activated, regardless whether the cause is a migrating thromboembolus or other material. The coagulation abnormality and, more importantly, the amount of ischemic injury resulting from microembolism was effectively reduced by factor XIIa inhibition, pointing to a novel treatment option to decrease the morbidity from SBI. The molecular imaging technologies used here allowed not only a better understanding of the biology of SBI, but may also have translational value to determine the severity of SBI in patients. The study further indicates that these molecular imaging strategies could be a sensitive tool to monitor therapeutic efficiency.

Supplementary Material

Refer to Web version on PubMed Central for supplementary material.

Acknowledgments

Funding

This work was supported by a grant from CSL Behring GmbH, and by grants from the NIH (grant numbers R01HL095629 and R01HL096576 to MN, R24-CA92782 to RW, R01-NS070835 and R01NS072167 to JWC).

We thank Dr. Weimer (CSL Behring GmbH) for providing rHA-Infestin-4.

Abbreviation list

SBI	silent brain ischemia
FXII	Factor XII

MPO	myeloperoxidase
Gd	gadolinium
DTPA	diethylenetriaminepentaacetate
MPO-Gd	bis-5-hydroxytryptamide-DTPA-Gd
SPECT	single photon emission computed tomography
CT	computed tomography
MRI	magnetic resonance imaging
DWI	diffusion weighted imaging
ROI	region of interest
TTC	2,3,5-triphenyltetrazolium chloride
CNR	contrast-to-noise ratio

References

1. Bendszus M, Stoll G. Silent cerebral ischaemia: hidden fingerprints of invasive medical procedures. Lancet Neurol. 2006; 5:364–72. [PubMed: 16545753]
2. Kim DE, Kim JY, Schellingerhout D, et al. Protease imaging of human atheromata captures molecular information of atherosclerosis, complementing anatomic imaging. Arterioscler Thromb Vasc Biol. 2010; 30:449–56. [PubMed: 20056915]
3. Vermeer SE, Longstreth WTJ, Koudstaal PJ. Silent brain infarcts: a systematic review. Lancet Neurol. 2007; 6:611–19. [PubMed: 17582361]
4. Vermeer SE, Hollander M, van Dijk EJ, Hofman A, Koudstaal PJ, Breteler MM. Silent brain infarcts and white matter lesions increase stroke risk in the general population: the Rotterdam Scan Study. Stroke. 2003; 34:1126–29. [PubMed: 12690219]
5. Davie EW. A brief historical review of the waterfall/cascade of blood coagulation. J Biol Chem. 2003; 278:50819–32. [PubMed: 14570883]
6. Colman RW. Biologic activities of the contact factors in vivo--potentiation of hypotension, inflammation, and fibrinolysis, and inhibition of cell adhesion, angiogenesis and thrombosis. Thromb Haemost. 1999; 82:1568–77. [PubMed: 10613636]
7. Chien P, Pixley RA, Stumpo LG, Colman RW, Schreiber AD. Modulation of the human monocyte binding site for monomeric immunoglobulin G by activated Hageman factor. J Clin Invest. 1988; 82:1554–59. [PubMed: 3263395]
8. Toossi Z, Sedor JR, Mettler MA, Everson B, Young T, Ratnoff OD. Induction of expression of monocyte interleukin 1 by Hageman factor (factor XII). Proc Natl Acad Sci U S A. 1992; 89:11969–72. [PubMed: 1465426]
9. Wachtfogel YT, Pixley RA, Kucich U, et al. Purified plasma factor XIIa aggregates human neutrophils and causes degranulation. Blood. 1986; 67:1731–37. [PubMed: 3486686]
10. Zabel BA, Allen SJ, Kulig P, et al. Chemerin activation by serine proteases of the coagulation, fibrinolytic, and inflammatory cascades. J Biol Chem. 2005; 280:34661–66. [PubMed: 16096270]
11. Schousboe I. Pharmacological regulation of factor XII activation may be a new target to control pathological coagulation. Biochem Pharmacol. 2008; 75:1007–13. [PubMed: 17996217]
12. Elkind MS, Cheng J, Rundek T, Boden-Albala B, Sacco RL. Leukocyte count predicts outcome after ischemic stroke: the Northern Manhattan Stroke Study. J Stroke Cerebrovasc Dis. 2004; 13:220–27. [PubMed: 17903979]
13. McColl BW, Rothwell NJ, Allan SM. Systemic inflammatory stimulus potentiates the acute phase and CXC chemokine responses to experimental stroke and exacerbates brain damage via interleukin-1- and neutrophil-dependent mechanisms. J Neurosci. 2007; 27:4403–12. [PubMed: 17442825]

14. Kleinschnitz C, Stoll G, Bendszus M, et al. Targeting coagulation factor XII provides protection from pathological thrombosis in cerebral ischemia without interfering with hemostasis. J Exp Med. 2006; 203:513–18. [PubMed: 16533887]
15. Renne T, Pozgajova M, Gruner S, et al. Defective thrombus formation in mice lacking coagulation factor XII. J Exp Med. 2005; 202:271–81. [PubMed: 16009717]
16. Schmaier AH. The elusive physiologic role of Factor XII. J Clin Invest. 2008; 118:3006–09. [PubMed: 18725991]
17. Hagedorn I, Schmidbauer S, Pleines I, et al. Factor XIIa inhibitor recombinant human albumin Infestin-4 abolishes occlusive arterial thrombus formation without affecting bleeding. Circulation. 2010; 121:1510–17. [PubMed: 20308613]
18. Muller F, Renne T. Novel roles for factor XII-driven plasma contact activation system. Curr Opin Hematol. 2008; 15:516–21. [PubMed: 18695377]
19. Campos IT, Tanaka-Azevedo AM, Tanaka AS. Identification and characterization of a novel factor XIIa inhibitor in the hematophagous insect, Triatoma infestans (Hemiptera: Reduviidae). FEBS Lett. 2004; 577:512–16. [PubMed: 15556638]
20. Bederson JB, Pitts LH, Tsuji M, Nishimura MC, Davis RL, Bartkowski H. Rat middle cerebral artery occlusion: evaluation of the model and development of a neurologic examination. Stroke. 1986; 17:472–76. [PubMed: 3715945]
21. Chen JW, Querol Sans M, Bogdanov AJ, Weissleder R. Imaging of myeloperoxidase in mice by using novel amplifiable paramagnetic substrates. Radiology. 2006; 240:473–81. [PubMed: 16864673]
22. Nahrendorf M, Sosnovik D, Chen JW, et al. Activatable magnetic resonance imaging agent reports myeloperoxidase activity in healing infarcts and noninvasively detects the antiinflammatory effects of atorvastatin on ischemia-reperfusion injury. Circulation. 2008; 117:1153–60. [PubMed: 18268141]
23. Breckwoldt MO, Chen JW, Stangenberg L, et al. Tracking the inflammatory response in stroke in vivo by sensing the enzyme myeloperoxidase. Proc Natl Acad Sci U S A. 2008; 105:18584–89. [PubMed: 19011099]
24. Tung CH, Ho NH, Zeng Q, et al. Novel factor XIII probes for blood coagulation imaging. Chembiochem. 2003; 4:897–99. [PubMed: 12964167]
25. Lyden PD, Zweifler R, Mahdavi Z, Lonzo L. A rapid, reliable, and valid method for measuring infarct and brain compartment volumes from computed tomographic scans. Stroke. 1994; 25:2421–28. [PubMed: 7974584]
26. Nahrendorf M, Hu K, Frantz S, et al. Factor XIII deficiency causes cardiac rupture, impairs wound healing, and aggravates cardiac remodeling in mice with myocardial infarction. Circulation. 2006; 113:1196–202. [PubMed: 16505171]
27. Jaffer FA, Tung CH, Wykrzykowska JJ, et al. Molecular imaging of factor XIIIa activity in thrombosis using a novel, near-infrared fluorescent contrast agent that covalently links to thrombi. Circulation. 2004; 110:170–76. [PubMed: 15210587]
28. Rodriguez E, Nilges M, Weissleder R, Chen JW. Activatable magnetic resonance imaging agents for myeloperoxidase sensing: mechanism of activation, stability, and toxicity. J Am Chem Soc. 2010; 132:168–77. [PubMed: 19968300]
29. Adams HPJ, del Zoppo G, Alberts MJ, et al. Guidelines for the early management of adults with ischemic stroke: a guideline from the American Heart Association/American Stroke Association Stroke Council, Clinical Cardiology Council, Cardiovascular Radiology and Intervention Council, and the Atherosclerotic Peripheral Vascular Disease and Quality of Care Outcomes in Research Interdisciplinary Working Groups: The American Academy of Neurology affirms the value of this guideline as an educational tool for neurologists. Circulation. 2007; 115:e478–534. [PubMed: 17515473]

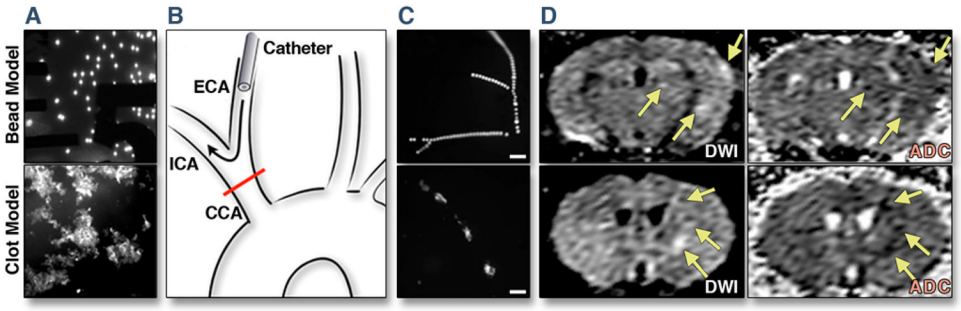

Figure 1. Model of SBI

(A) Fluorescent microbeads and fractionated fluorescent thromboemboli prior to injection. (B) Surgical approach with catheter retrogradely inserted into the external carotid artery (ECA). During injection, the common carotid artery (CCA) was temporarily ligated to force the embolic material into the internal carotid artery (ICA). (C) Ex vivo fluorescence images of the brain surface after injection of either microbeads or thromboemboli, scale bar indicates 200μm. (D) Diffusion weighted MRI was done 4 hours after embolism and shows hallmarks of SBI similar to what is seen in patients. Multiple small lesions (some marked by arrows) are revealed by diffusion weighted imaging (DWI). Decrease in the apparent diffusion coefficient (ADC) in the corresponding areas confirmed restricted diffusion, characteristic of acute infarcts.

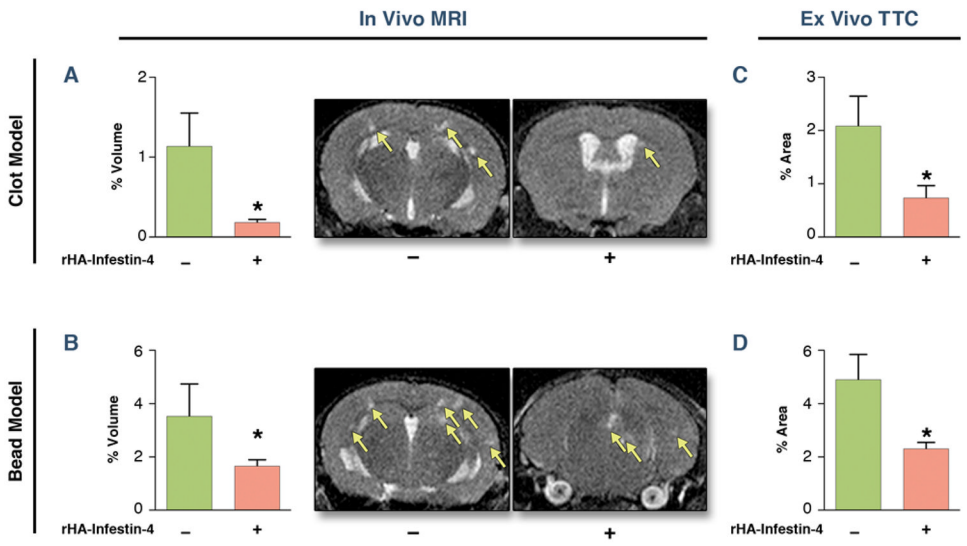

Figure 2. rHA-Infestin-4 reduces injury quantified by MRI and TTC on day 3 after SBI

(A, B) Assessment of infarct volume by T2 MRI on day 3 after SBI (Mann-Whitney U test). (C, D) Assessment of tissue damage by TTC staining on day 3 after SBI. Figure shows bar graphs, and representative MRI. Data are presented as mean ± SEM. * $p < 0.05$.

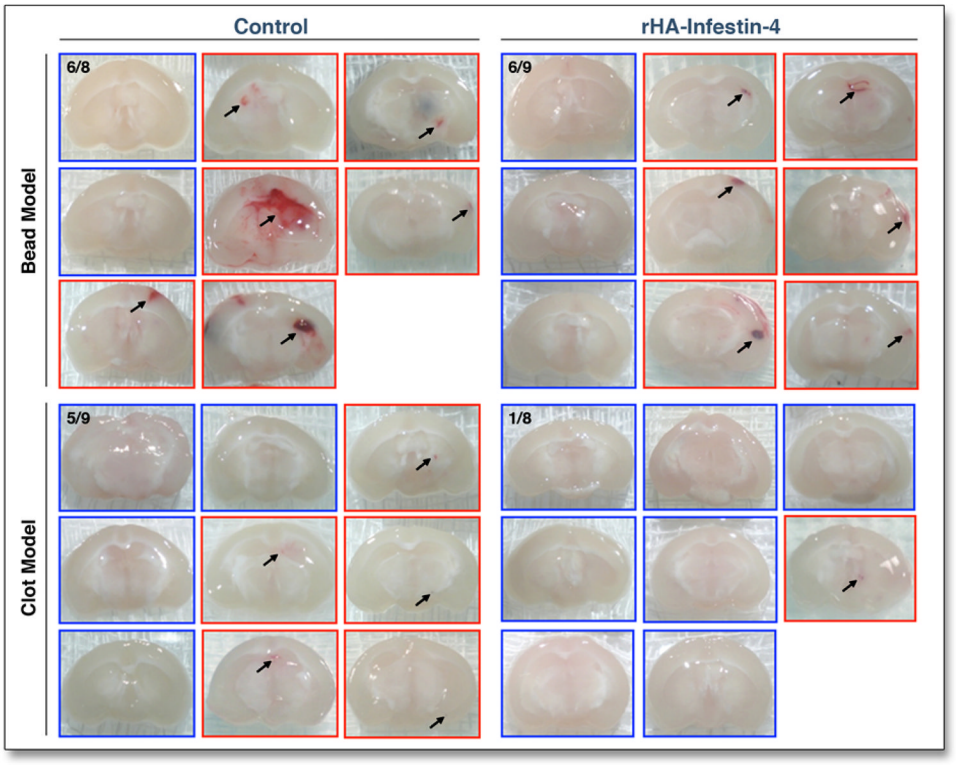

Figure 3. Secondary hemorrhage is not increased by rHA-Infestin-4

Assessment of secondary hemorrhage on day 3 after injection of microbeads or thromboemboli. One representative brain slice is shown per mouse. Red frames indicate mice in which hemorrhage was detected (arrows).

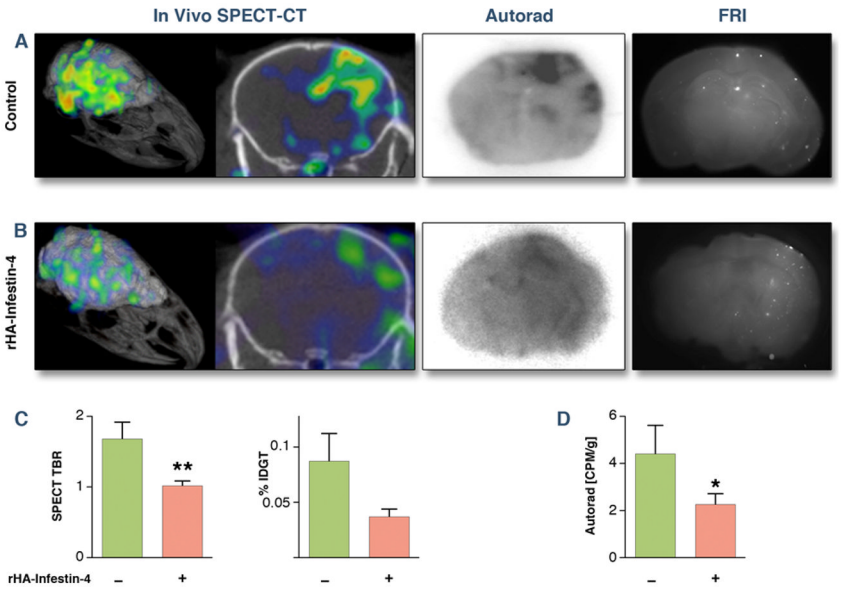

Figure 4. rHA-Infestin-4 reduces clotting in thromboemboli-induced SBI

(A) Assessment of transglutaminase activity (FXIIIa) 3 hours after application of thromboemboli by SPECT-CT, autoradiography, and fluorescence reflectance imaging (FRI). (B) After rHA-Infestin-4 administration. (C) Quantification of SPECT target to background ratio (TBR), ex vivo scintillation counting of entire brain (Mann-Whitney U test). Data are shown as percent injected dose per gram tissue (%IDGT). (D) quantification of autoradiography (CPM: counts per minute). Data are presented as mean ± SEM. * $p < 0.05$.

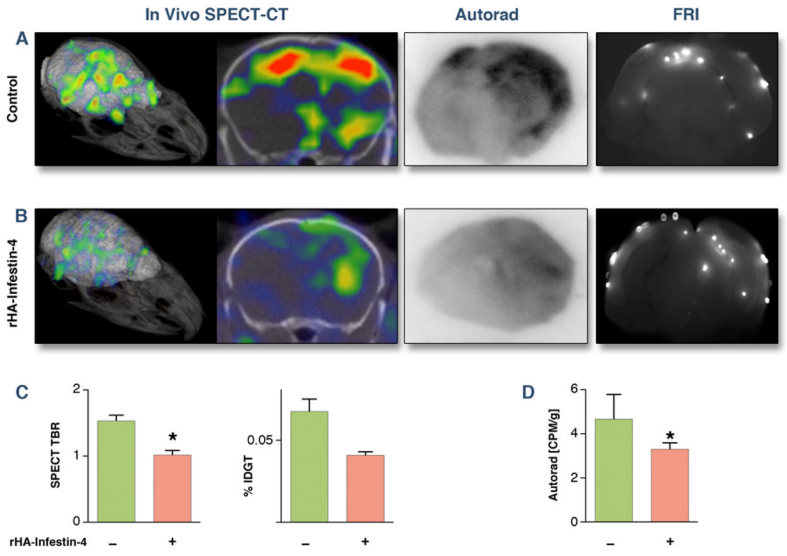

Figure 5. rHA-Infestin-4 reduces clotting in microbead-induced SBI

(A) Assessment of transglutaminase activity (FXIIIa) 3 hours after application of microbeads by SPECT-CT, autoradiography, and fluorescence reflectance imaging (FRI). (B) After rHA-Infestin-4 administration. (C) quantification of SPECT target to background ratio (TBR) and ex vivo scintillation counting of entire brain (Mann-Whitney U test). Data are shown as percent injected dose per gram tissue (%IDGT). (D) quantification of autoradiography (CPM: counts per minute). Data are presented as mean ± SEM. * $p < 0.05$.

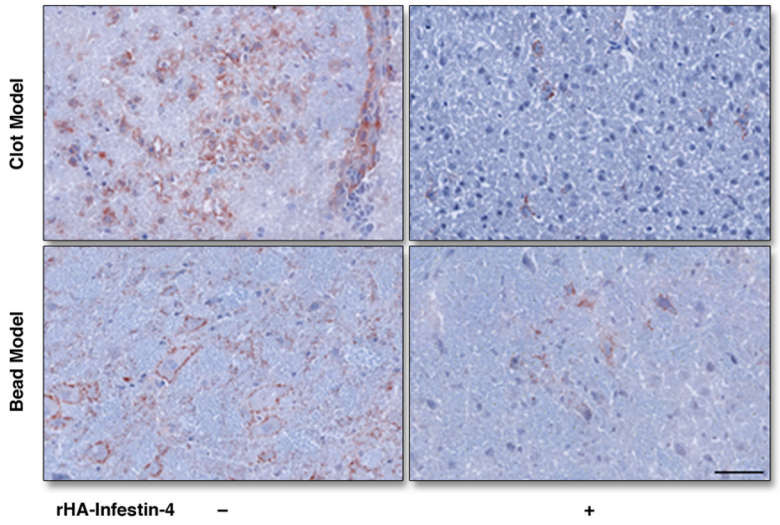

Figure 6. Immunohistochemistry for FXIII

Immunohistochemical staining for FXIII, 3 hours after induction of SBI. Bar indicates 50 μm.

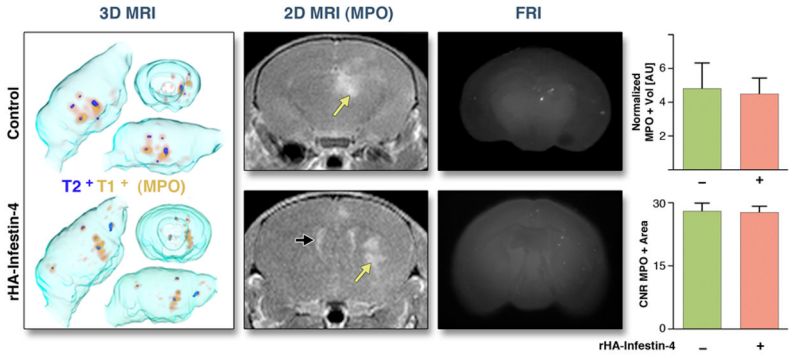

Figure 7. MR imaging of MPO activity on day 3 after thromboemboli-induced SBI

Assessment of MPO activity 3 days after SBI induced by thromboemboli. Yellow arrows point at MPO^+ lesions, black arrows at ventricle. FRI: Fluorescence reflectance imaging, showing location of thromboemboli. MPO+ volume is normalized to T2+ volume. CNR: Contrast-to-noise-ratio. AU: Arbitrary units. Data are presented as mean ± SEM.

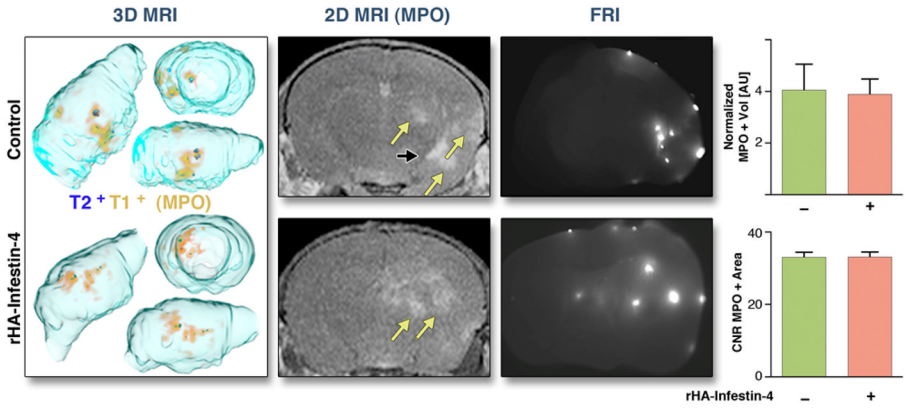

Figure 8. MR imaging of MPO activity on day 3 after microbead-induced SBI

Assessment of MPO activity 3 days after SBI after microbead embolism. Yellow arrows point at MPO^+ lesions, black arrows at ventricle. FRI: Fluorescence reflectance imaging, showing position of beads. MPO+ volume is normalized to T2+ volume. AU: Arbitrary units. CNR: Contrast-to-noise-ratio. Data are presented as mean ± SEM.